Biophysical Reports, Volume *2*

Supplemental information

KHz-rate volumetric voltage imaging of the whole Zebrafish heart

Leonardo Sacconi, Ludovico Silvestri, Esteban C. Rodríguez, Gary A.B. Armstrong, Francesco S. Pavone, Alvin Shrier, and Gil Bub

Supplementary Information for 'KHz-rate volumetric voltage imaging of the whole zebrafish heart'

Supplemental Movie S1a: Video showing propagation through the atria, AV canal region and ventricles, imaged at 500 Hz. The volume imaged corresponds to a 250x250x250 μm cube of the spontaneously beating zebrafish heart.

Supplemental Movie S1b: Video showing images captured by the system as viewed using the control software. Data from the seven cameras are aggregated so that a single frame contains seven side-by-side images. The first part of the video shows the raw data. This is followed a view where single frame from this aggregate image is subtracted from the rest, and the data rescaled to visualize the depolarization wave.

Design considerations: The system was designed to equally divide the emission light to different detection paths in the microscope. The tolerances of the 50:50 beam-splitters were checked using constant LED illumination and moving a single camera to different paths. We found that the average intensity over the entire frame varied by 1.5% in different detection paths of the microscope. However, we also found different cameras display variation in intensity readings at the same settings, likely caused by variability in internal digitizing components within each camera. The average pixel intensity values under constant illumination display a relative standard deviation of 18.6% between cameras. This variation can be reduced by adjusting the gain setting (between 0 and 5 dB out of a maximum allowed value of 33 dB) for each camera using the 'camera.Gain.SetValue' function supplied by Pylon SDK. After adjustment, the seven cameras display average pixel intensities that vary by relative standard deviation of 2.2%. Adjusting the gain in principle adds a small amount of noise but in practice we find that this is less than the shot noise: under constant illumination, the pixel intensity over 100 frames has an average relative standard deviation before and after adjustment of 1.038 and 1.034% respectively.

The seven cameras are connected to a single computer using two Fresco FL1100 USB 3.0 cards, which have four USB ports each. The computer also controls an Arduino board, which was programmed to send TTL level pulses to the cameras. The cameras are specified by the manufacturer to respond within 15 microseconds to a TTL pulse, which is sufficient to ensure millisecond accuracy when measuring events captured by different sensors.

High resolution scanning: The microscope can also be operated as a conventional scanning light-sheet microscope, by blocking all but one excitation plane and moving the sample relative to the light-sheet. Our prototype used a Thorlabs Z812B motorized actuator attached to the sample holder stage, where the actuator is controlled by a Thorlabs KDC101 Cube controller. The controller is set to move the sample at a constant speed (0.025mm/sec) while imaging the sample at a constant rate (20Hz), resulting in a spacing between frames of 1.25 μm. This was done to capture high resolution structural data in Figure 2b.

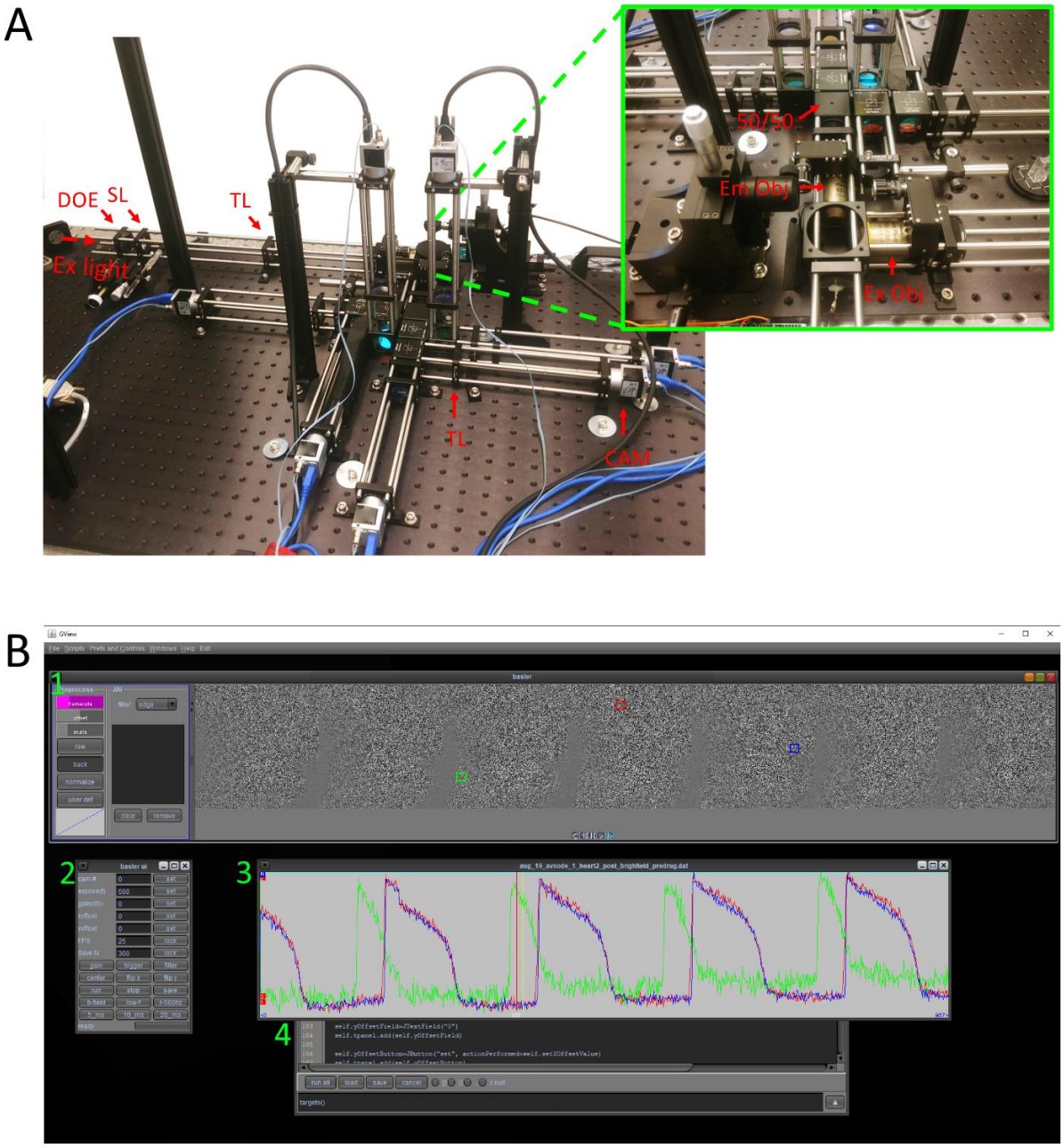

Supplemental Figure S2: A) Image of the SPEED microscope, showing the excitation and emission objectives (Ex Obj and Em Obj) the seven cameras (CAM), tube lenses (TL), diffractive optical element (DOE), scan lens (SL) and light path. The system is constructed using standard Thorlabs beam splitting cubes and 30mm cage components. The inset shows the imaging area with orthogonally placed objectives and a series of 50/50 beam splitting cubes. See Figure 1 (main text) for details. B) Screenshot of the computer program (GView) that controlled the SPEED microscope: 1) The camera viewing window showing the camera views side-by-side after a frame subtract operation; 2) the control interface; 3) Intensity vs time plots of the regions of interest (ROIs) shown by the colored squares in the view window; 4) the Jython scripting window and command line interface. The software is available for download here: http://dx.doi.org/10.5281/zenodo.5800192.

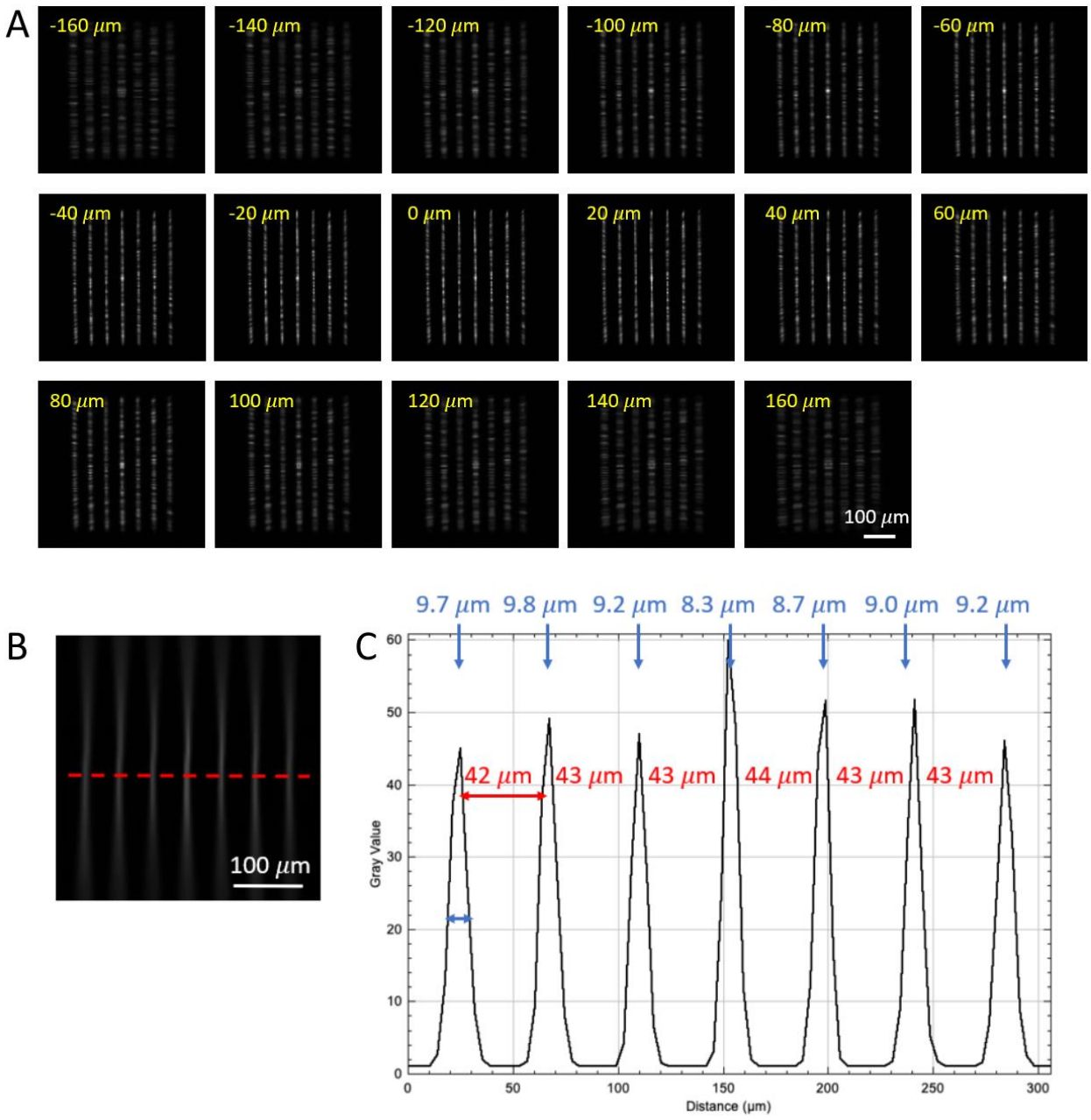

Supplemental Figure S3: A) Seven light sheets acquired after the excitation objective using an image sensor placed on planes perpendicular to the propagation axis. In yellow is the displacement of the detection plane with respect to the waist position. B) Top view projection of seven light sheets measured after the excitation objective lens. C) The plot intensity profile on the light-sheet waist highlights the distance between each plane (in red) and the thickness (in blue) of each light-sheet waist.

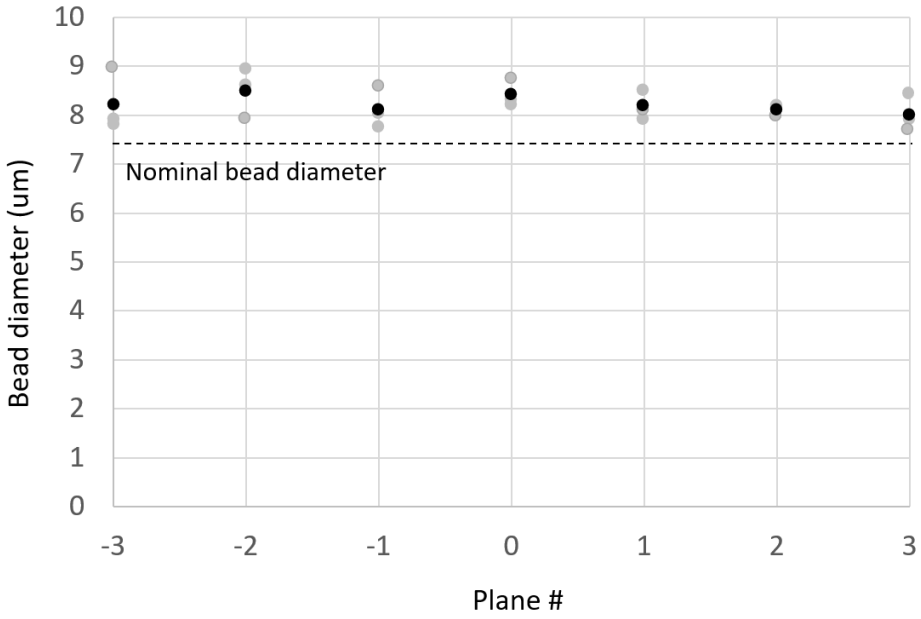

Figure S4: Measurement of fluorescent bead diameter across the seven planes. For each recording, only the plane in focus was illuminated with the associated light sheet. We report three measurements per plane in grey and in the mean value in black. For comparison, the nominal bead diameter is also shown in the graph. The fluorescent beads used in this study (Bangs Laboratories Inc. catalog #FSFR007) have a diameter of 7.32 μm.

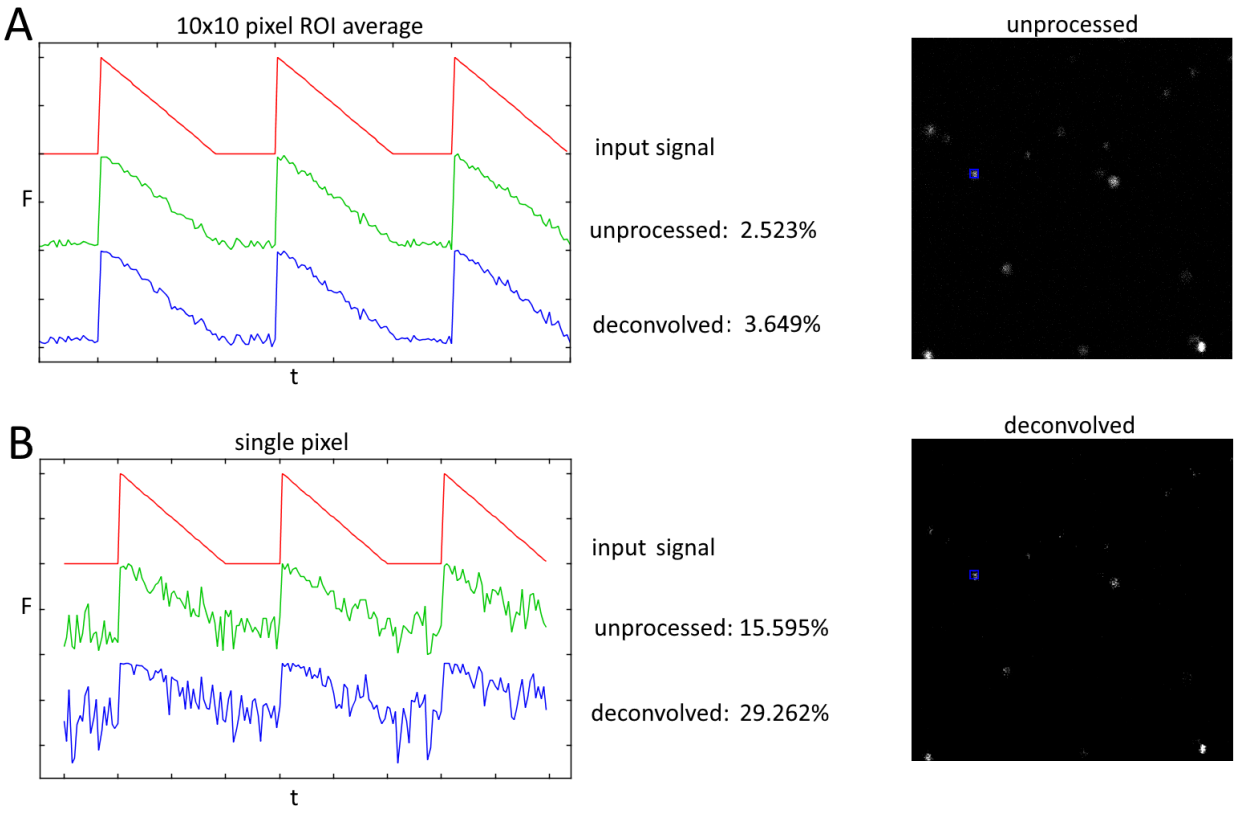

Supplemental Figure S5: The effects of deconvolution on wavefront reconstruction were estimated by superimposing an idealized action potential transient (red trace in panels A and B) on captured videos of fluorescent beads (right panels). The imposed signal amplitude is adjusted to approximate the signal to noise of real fluorescent voltage signals (e.g., see Figure 2E). Traces before (green: unprocessed) and after (blue: deconvolved) deconvolution are shown for a 10x10 region of interest (panel A) and a single pixel within that region of interest (panel B). The noise is quantified by finding the average absolute value difference between the input signal and the simulated data and dividing it by the action potential amplitude for the traces shown in A and B. Deconvolution adds noise but activation times can still be obtained after moderate spatial averaging.

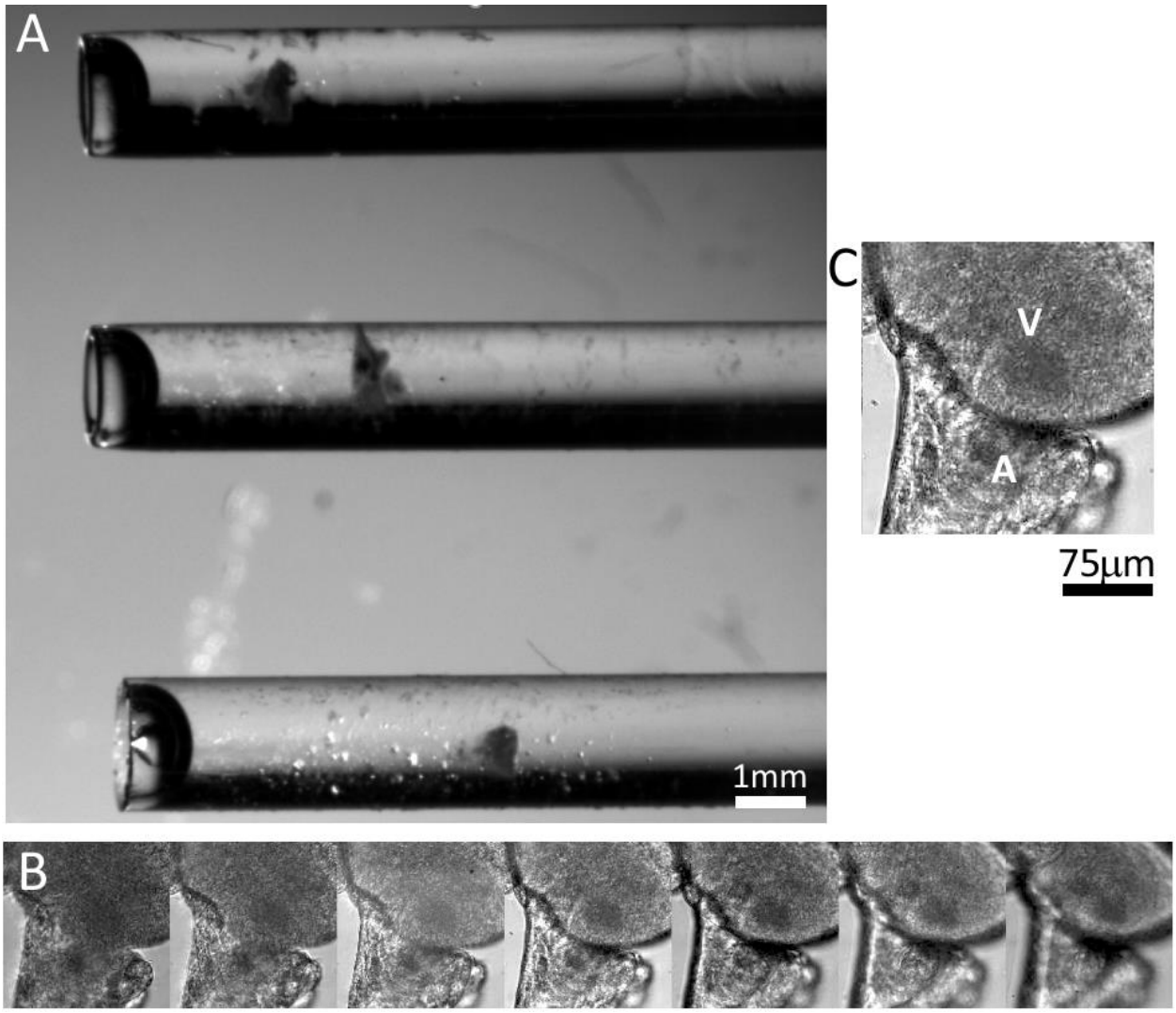

Supplemental Figure S6: Image of three extracted zebrafish hearts in capillary tubes. B) Brightfield (LED illuminated) images of a zebrafish heart as captured by the SPEED microscope. C) Brightfield image of a zebrafish heart from a single camera showing the ventricles ('V') and atria ('A').\

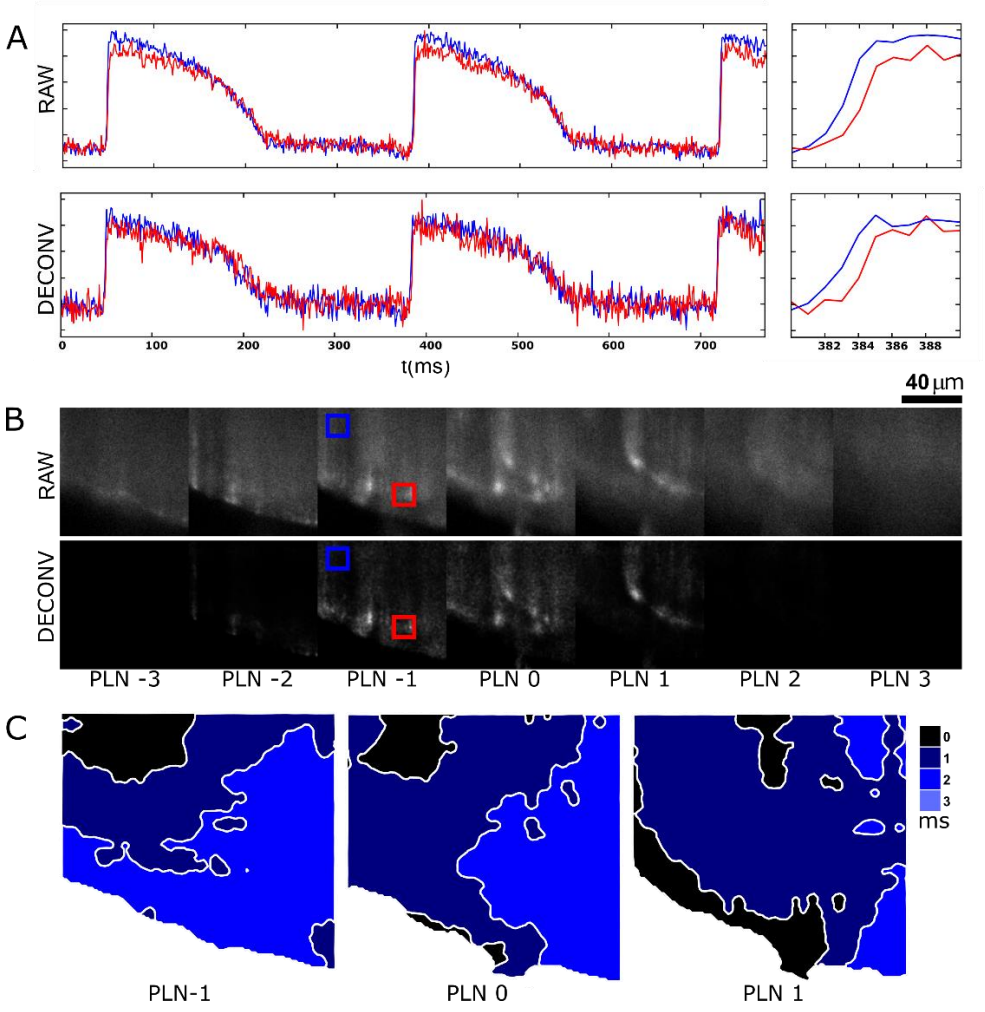

Supplemental Figure S7: 1000 f/s (KHz-rate) imaging of ventricular tissue. 128x128 pixel region was selected to image propagation across the ventricle at high speeds. Intensity vs time traces (panel A) show propagation across the field occurs over approximately 2ms, for both the raw and deconvolved signal. Deconvolution (panel B, bottom) resulted in a redistribution of signal to three out of the seven frames. Isochronal maps from the three central planes suggests that the wave propagates in both radially and axially.

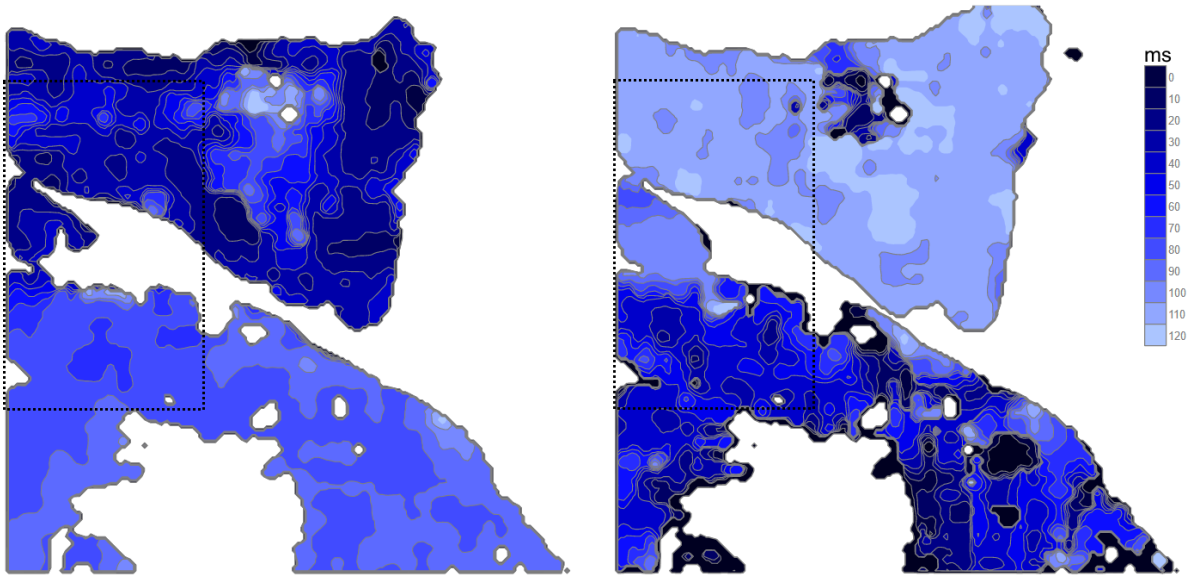

Supplemental Figure S8: Isochronal maps at two time points for a 250 x 250 μm region showing propagation during EAD dynamics for the first atrial beat, where the impulse originates in the atria and propagates via the AV canal to the ventricle (left panel), and for subsequent EAD beats, where the impulse originates in the ventricle and propagates retrogradely through the AV canal to activate the atria. The dashed line insets show the regions depicted in Figure 3g in the main text. Isochronal maps for EAD retrograde propagation were obtained by averaging signals from two adjacent cameras and averaging three successive EADs.